

# Surface and Interface Properties in Thin-Film Solar Cells: Using Soft X-rays and Electrons to Unravel the Electronic and Chemical Structure

Lothar Weinhardt,\* Dirk Hauschild,\* and Clemens Heske\*


Thin-film solar cells have great potential to overtake the currently dominant silicon-based solar cell technologies in a strongly growing market. Such thin-film devices consist of a multilayer structure, for which charge-carrier transport across interfaces plays a crucial role in minimizing the associated recombination losses and achieving high solar conversion efficiencies. Further development can strongly profit from a high-level characterization that gives a local, electronic, and chemical picture of the interface properties, which allows for an insight-driven optimization. Herein, the authors' recent progress of applying a "toolbox" of high-level laboratory- and synchrotron-based electron and soft X-ray spectroscopies to characterize the chemical and electronic properties of such applied interfaces is provided. With this toolbox in hand, the activities are paired with those of experts in thin-film solar cell preparation at the cutting edge of current developments to obtain a deeper understanding of the recent improvements in the field, e.g., by studying the influence of so-called "post-deposition treatments", as well as characterizing the properties of interfaces with alternative buffer layer materials that give superior efficiencies on large, module-sized areas.

## 1. Introduction

One of the most pressing problems of today's society is to meet the growing demand for readily available energy sources. To fulfill this demand while avoiding the problems associated with

Dr. L. Weinhardt, Dr. D. Hauschild, Prof. C. Heske  
Institute for Photon Science and Synchrotron Radiation (IPS)  
and Institute for Chemical Technology and Polymer Chemistry (ITCP)  
Karlsruhe Institute of Technology (KIT)  
Hermann-v.-Helmholtz-Platz 1  
76344 Eggenstein-Leopoldshafen, Germany  
E-mail: Lothar.Weinhardt@kit.edu; Dirk.Hauschild@kit.edu;  
heske@kit.edu

Dr. L. Weinhardt, Prof. C. Heske  
Department of Chemistry and Biochemistry  
University of Nevada Las Vegas (UNLV)  
4505 Maryland Parkway, Las Vegas  
NV 89154-4003, USA

 The ORCID identification number(s) for the author(s) of this article can be found under <https://doi.org/10.1002/adma.201806660>.

© 2019 The Authors. Published by WILEY-VCH Verlag GmbH & Co. KGaA, Weinheim. This is an open access article under the terms of the Creative Commons Attribution-NonCommercial-NoDerivs License, which permits use and distribution in any medium, provided the original work is properly cited, the use is non-commercial and no modifications or adaptations are made.

DOI: 10.1002/adma.201806660

fossil or nuclear energy, strong efforts are undertaken to exploit renewable energy sources. In particular, the abundance of solar power makes it an attractive candidate. While silicon-based photovoltaics still dominate the market, thin-film solar cells promise reduction in material and energy input, ease of manufacturing, and ultimately cost reduction. Significant progress has been made over the last two decades, and thin-film solar cells now have reached efficiencies close to 23% on the laboratory scale (22.9% for cells based on Cu(In,Ga)(S,Se)<sub>2</sub><sup>[1]</sup> (CIGSSe) and 22.1% for cells based on CdTe<sup>[1]</sup>) and large areas (CIGSSe 19.2%<sup>[1]</sup> and CdTe 18.6%<sup>[1]</sup>).

The latest significant advance for CIGSSe solar cells was achieved with the introduction of a "post-deposition treatment" (PDT),<sup>[2]</sup> which is applied to the solar absorber surface. In many (but not all) cases, such PDTs led to a significant improvement in power conversion efficiency, resulting in several new world records.<sup>[2–4]</sup> For outstanding device performance, the properties of the internal interfaces are crucial for charge separation, electron transport, and (minimized) recombination losses, all of which are governed by the electronic (e.g., band alignment and the positions of valence band maximum, VBM, and conduction band minimum, CBM, relative to the Fermi level) and chemical (e.g., intermixing, secondary phases) structure at these interfaces. At the same time, thin-film solar cells are very complex, comprised of a multitude of layers, interfaces, surfaces, grain boundaries, elements, and impurities, and their properties sensitively depend on the exact process parameters during a substantial number of processing steps.

Figure 1 shows a (simplified) layer structure of a CIGSSe thin-film solar cell. Photons illuminate the cell from the side of the transparent front contact, penetrate through the buffer layer, and are absorbed in the absorber film. Subsequently, the generated charge carriers are separated by the built-in electric field between absorber and buffer, the electrons traveling to the front contact, and the holes to the back contact. Such structures have been mostly optimized empirically, with substantial support from the characterization and theory communities, and can increasingly profit from further (and increasingly more powerful) in-depth analysis, which allows for a further deliberate optimization and control of the applied modifications.

Figure 1 shows a (simplified) layer structure of a CIGSSe thin-film solar cell. Photons illuminate the cell from the side of the transparent front contact, penetrate through the buffer layer, and are absorbed in the absorber film. Subsequently, the generated charge carriers are separated by the built-in electric field between absorber and buffer, the electrons traveling to the front contact, and the holes to the back contact. Such structures have been mostly optimized empirically, with substantial support from the characterization and theory communities, and can increasingly profit from further (and increasingly more powerful) in-depth analysis, which allows for a further deliberate optimization and control of the applied modifications.

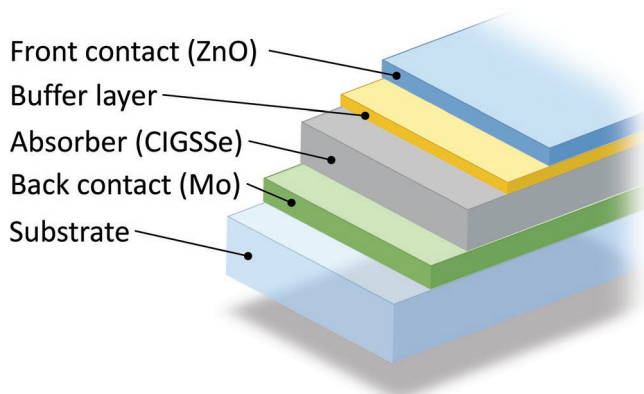


**Figure 1.** Simplified layer structure of a CIGSSe thin-film solar cell. Layer thicknesses are not to scale.

In this paper, we summarize our recent progress in applying cutting-edge lab- and synchrotron-based electron and soft X-ray spectroscopy techniques to study the electronic and chemical structures of surfaces and interfaces in thin-film solar cells. The particular power of this approach lies in combining several experimental techniques and their specific strengths to derive a very detailed picture of the respective properties, which is fed back to the device and process development for further optimization.

Section 2 gives a brief overview of the spectroscopic techniques, while Section 3 focuses on the characterization of the *chemical* interface structure. Section 4 discusses the *electronic* interface structure. The examples in these two sections focus on two of the most relevant recent developments for CIGSSe thin-film solar cells: 1) the introduction of alkali fluoride PDTs, which has led to a significant efficiency increase, and 2) the successful development of  $\text{In}_2\text{S}_3$  as an alternative, Cd-free buffer layer that can be integrated in a dry inline production line and yields the highest efficiency modules.<sup>[1]</sup>

## 2. Electron and Soft X-ray Spectroscopy Techniques

Electron and soft X-ray spectroscopies are powerful techniques for the investigation of the chemical and electronic structures of materials. Using a combination of various techniques that probe different aspects of the electronic and chemical structures and have different surface sensitivity, a detailed picture of the surface and the surface-near bulk can be obtained. And, in particular, when combined with a suitably chosen set of samples (e.g., of increasing overlayer thickness), it is possible to derive a comprehensive description of interfaces and multilayer structures.

The toolbox of techniques employed here includes X-ray and UV photoelectron spectroscopy (XPS and UPS), inverse photoemission spectroscopy (IPES), and X-ray excited Auger electron spectroscopy (XAES), representing the lab-based techniques. As synchrotron-based methods, soft X-ray absorption spectroscopy (XAS), soft X-ray emission spectroscopy (XES), and their resonantly excited combination (resonant inelastic soft X-ray scattering, RIXS) are employed. In all of these



**Lothar Weinhardt** received his Dr. rer. nat. in 2005 from the University of Würzburg, Germany. After postdoc stays at the Universities of Nevada, Las Vegas (UNLV) and Würzburg, he joined the Karlsruhe Institute of Technology (KIT) as head of the department for X-ray spectroscopy at the Institute for Photon Science and Synchrotron Radiation. He is also an Adjunct Associate Professor at UNLV. His current research focuses on the application and development of electron and soft X-ray spectroscopies for the study of energy materials (including in situ and operando), as well as fundamental studies of gases, liquids, and biological solutions.



**Dirk Hauschild** earned his Diploma (2011) and Dr. rer. nat. (2016) in Physics from the University of Würzburg, Germany. He then joined the Institute for Chemical Technology and Polymer Chemistry (ITCP) and the Institute for Photon Science and Synchrotron Radiation (IPS) at the Karlsruhe Institute of Technology (KIT) as a postdoctoral fellow. His research focuses on the investigation of surfaces and interfaces in applied material systems, with particular focus on thin-film solar cells.



**Clemens Heske** is a Professor for Applied Spectroscopy at the Institute for Chemical Technology and Polymer Chemistry (ITCP) at the Karlsruhe Institute of Technology (KIT) since 2011. He also serves as director of KIT's Institute for Photon Science and Synchrotron Radiation (IPS) and Professor at the Chemistry Department of the University of Nevada, Las Vegas (UNLV, since 2004). He received his doctorate from the University of Würzburg, Germany (1996), worked as a post-doctoral fellow and beamline scientist at the Advanced Light Source (Berkeley Lab), and completed his Habilitation in Experimental Physics at the University of Würzburg in 2004.

spectroscopic techniques, X-rays and/or electrons interact with the electronic structure of the sample, as schematically depicted in **Figure 2**.

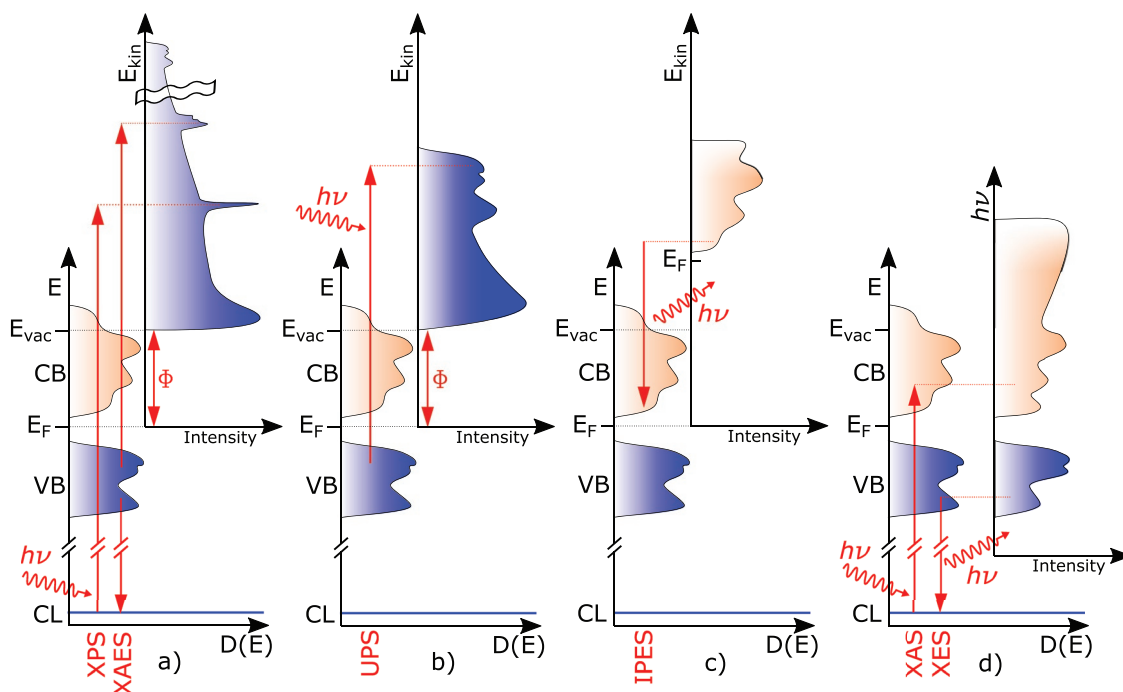


**Figure 2.** Schematic diagram depicting a) XPS and XAES, b) UPS, c) IPES, and d) XAS and XES (left: ground-state electronic structure, and right: simplified spectrum). “D(E)” denotes the energy-dependent density of states, “ $E_{\text{vac}}$ ” the vacuum level, and “ $E_{\text{F}}$ ” the Fermi level. “CL” denotes a representative core level, “VB” the valence band, “CB” the conduction band, and “ $\Phi$ ” the work function. Blue and beige shading, respectively, indicate occupied and unoccupied electronic states, as well as their corresponding spectra. Vertical red arrows represent excitations and de-excitations of electrons into unoccupied electronic states/holes.

In XPS (or UPS), the sample is excited by an X-ray (or UV) photon with energy  $h\nu$ , emitting an electron (the “photoelectron”) from an occupied electronic state (Figure 2 a, b). The number of photoelectrons emitted from the sample is recorded as a function of kinetic energy  $E_{\text{kin}}$  (or binding energy  $E_{\text{B}} = h\nu - E_{\text{kin}}$ ), resulting in a photoemission spectrum. Both XPS and UPS are very surface-sensitive techniques due to the short inelastic mean-free path of the photoelectrons (defined as the  $1/e$  attenuation length), in the order of 1–3 nm<sup>[5,6]</sup> for excitation in the UV and soft X-ray range. With XPS, usually the core levels are probed, which give information about the elemental composition at the surface as well as the chemical environment of a respective element. With UPS, the occupied valence states are probed, which (in particular) allows deriving the energetic position of the VBM of a semiconductor relative to the Fermi level.

For IPES, the sample is illuminated with (slow) electrons that relax into unoccupied electronic states, emitting UV photons as depicted in Figure 2c. By scanning the initial electron energy and detecting UV photons of a fixed photon energy, information on the conduction band can be obtained and, in particular, the position of the CBM of a semiconductor with respect to the Fermi level can be determined.

For XAES, a core hole (created by, e.g., an X-ray absorption process) is filled while emitting an electron of a characteristic kinetic energy. This is also sketched in Figure 2a and is measured as part of the XPS data (or vice versa). The spectra contain detailed information about elements and their chemical bonds present at the surface, complementary to XPS.

While for the techniques above, a laboratory setup can be used, XAS, XES, and RIXS need to be performed at a synchrotron light source that provides X-rays with very high flux and/or brightness, small energy band width, and “tunable” photon energy.

In XAS, the sample is illuminated with X-rays and their energy is scanned across an absorption edge. In a one-electron picture (as sketched in Figure 2d), an electron from a core level is then excited into an *unoccupied* electronic state. For semiconductors, the spectra contain valuable information about the conduction band and the chemical environment of the probed atoms, which can be selected by choosing the corresponding absorption edges. Depending on the setup and purpose of the experiments (e.g., the desire for high or low surface sensitivity), specific “yield” modes are chosen, for which most commonly electrons or X-rays emitted from the sample are detected as a function of exciting photon energy.

In competition to the Auger process described above, a core hole can also be filled with a valence electron while emitting an X-ray photon (Figure 2d). In XES, the emitted X-ray photons are detected with a high-resolution X-ray spectrometer,<sup>[7,8]</sup> giving a spectrum of the *occupied* valence states from the viewpoint of the selected core hole. These spectra contain information on a multitude of different aspects, including core–hole and symmetry effects. For the applied systems studied here, the insight into the local bonding environment provided by XES is of particularly high value, as will be shown below.

Our experiments are conducted in the Materials For Energy lab at the KIT, surface science labs at the University of

Würzburg (Experimentelle Physik VII), and UNLV, the X-SPEC beamline at KIT's KARA electron storage ring, and the SALSA and iRIXS end stations at Beamline 8.0.1<sup>[8,9]</sup> at the Advanced Light Source (ALS), Lawrence Berkeley National Laboratory.

### 3. The Chemical Structure of Thin-Film Solar Cell Surfaces and Interfaces

While ultimately solar cell development focuses on power conversion efficiency, device stability, and cost, a detailed understanding of the chemical structure at the surfaces and interfaces of the device and their relation to the electronic structure (and ultimately the cell performance parameters) is the key for a deliberate and insight-driven optimization.

It is well established that the chemical properties at the surface of CIGS<sub>Se</sub> thin-film solar cells deviate from the properties of the bulk. The surface is found to have a copper-poor stoichiometry,<sup>[10–13]</sup> causing a widening of the bandgap at the surface,<sup>[10–12,14–16]</sup> which is a key property of high-efficiency devices. In general, good absorber films exhibit empirically or deliberately formed gradients in composition, which, if controlled properly, can be used for device optimization. In addition, originally unintended elements are found on the absorber surface, e.g., sodium.<sup>[17–20]</sup> Sodium originally diffused from the soda-lime glass, through back contact and absorber, to the absorber surface. It was found to be necessary to achieve high efficiencies, as it helps to form large crystallites,<sup>[17]</sup> increases conductivity of the film,<sup>[21]</sup> and also plays an important role at the surface of the absorber and at its interface to the buffer layer.<sup>[18–20,22,23]</sup> The idea of the recently introduced alkali PDT of the absorber surface runs along these lines, leading to a further optimization of the absorber surface and the absorber/buffer layer interface, as will be discussed in the following.

Over the last few years, we have studied the influence of the alkali PDT for samples from different partners, both in research as well as industrial environments.<sup>[24–27]</sup> While some general effects can be observed, we find that the effect of the alkali PDT differs for different manufacturers, which is likely caused by different initial absorber compositions and/or preparation procedures. In the following, we will discuss spectra of samples from the Zentrum für Sonnenenergie- und Wasserstoff-Forschung Baden-Württemberg (ZSW) before and after alkali PDT as an example. While the alkali PDT was originally introduced by the Swiss Federal Laboratories for Materials Science and Technology (Empa) using KF,<sup>[2]</sup> ZSW has been very successful with heavier alkali metals, leading to a world-record efficiency with an RbF PDT<sup>[3]</sup> (only recently surpassed by Solar Frontier<sup>[4]</sup> using a more complicated alkali incorporation approach).

The XPS survey spectra of ZSW absorber samples before and after RbF PDT are presented in **Figure 3**. The peak intensities of the Ga, In, and Se lines remain constant after PDT, and a quantification shows no changes in the Ga/(Ga+In) (GGI) ratio.<sup>[27]</sup> This is different from the effect of the KF PDT on the Empa absorber surface, where the data suggest an almost complete removal of Ga from the surface,<sup>[2,26]</sup> and from the Stion (industrial) line, where the KF PDT leads to a substantial surface cleaning and a significant increase in the intensity of all Ga XPS and Auger lines after PDT.<sup>[25]</sup>

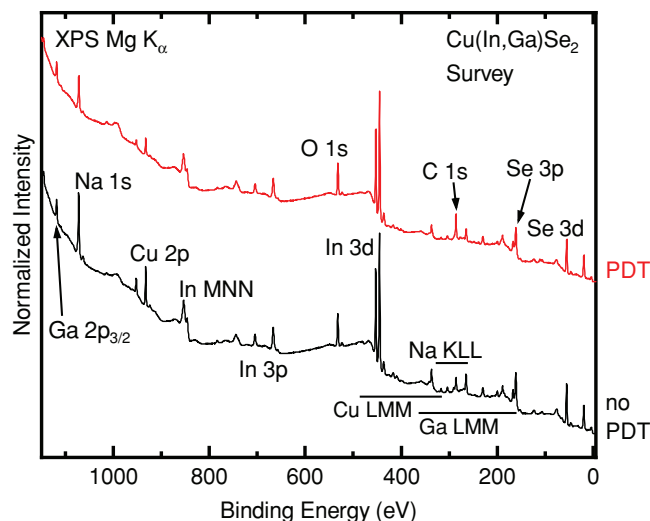


**Figure 3.** Mg  $K_{\alpha}$  XPS survey spectra for CIGSe before (black) and after RbF-PDT (red).

Different from the behavior of Ga, In, and Se, we find a strong reduction of the Cu 2p signal on the ZSW absorber surface after RbF PDT. This is in accordance with other studies observing such a reduction in Cu content at the CIGS<sub>Se</sub> surface after KF PDT,<sup>[25,28,29]</sup> but in contrast to studies suggesting a complete KF PDT-induced removal of Cu from the surface.<sup>[2,26,30]</sup> Besides these changes of the surface stoichiometry, K<sup>[2,25]</sup> or (in the ZSW case) Rb<sup>[27]</sup> is observed on the absorber surface after PDT, while a reduction of Na occurs (see Figure 3 and refs. <sup>[25,27]</sup>).

A careful evaluation of the XPS and XAES detail spectra gives further information, painting a very detailed picture of the chemical properties at the surface. Exemplarily, **Figure 4** shows the In and Ga XAES spectra of the ZSW absorber surface (“0 s CdS”) before and after RbF PDT, as well as after 2 s in the chemical bath used for deposition of the CdS buffer layer (“2 s CdS”). In general, XAES spectra are comprised of a multitude of transitions, which lead to more complex spectral shapes as compared to XPS. Still, if this spectral shape is known (e.g., from suitable references), the spectra of the sample can be analyzed with respect to different chemical species, as is done in Figure 4. As expected, most of the In and Ga atoms are found in a Cu(In,Ga)Se<sub>2</sub> environment, but also a significant oxide component is observed. This oxide component does increase after PDT treatment, but is reduced (for In) and fully removed (for Ga) after 2 s in the chemical bath, which can likely be attributed to an etching effect of the ammonia in the solution.

A quantitative analysis of the absorber line intensities as a function of chemical bath time with and without PDT<sup>[27,33]</sup> allows us to draw conclusions about the growth of the CdS film. We find that the CdS film grows denser and more homogeneous on the absorber *with* PDT. This allows to use effectively thinner buffer layers (and reduce the chemical bath time), which in turn reduces the absorption losses in this layer.<sup>[33]</sup>

We thus find the RbF PDT to influence the stoichiometry at the surface: The alkali metals from the PDT are incorporated into the absorber surface, Cu is partly (or even fully) removed from the surface, and the concentration of Ga at the surface



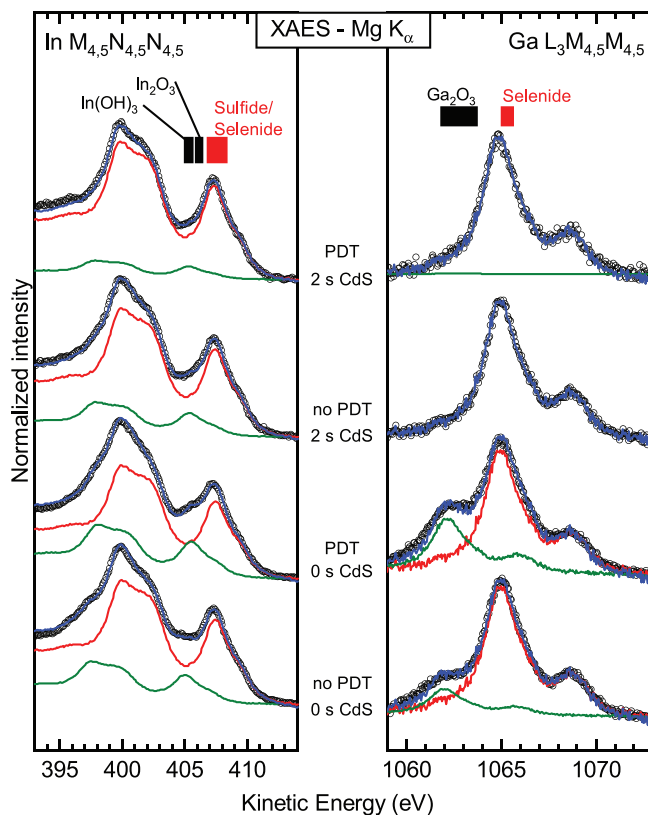


**Figure 4.** Mg  $K_{\alpha}$ -excited XAES spectra of indium (left) and gallium (right) for the two bare absorbers (two bottom spectra) and the samples with 2 s CdS chemical bath deposition (two uppermost spectra). Raw data are represented as open black circles, individual species (fit components) are represented in green and red colors, and the sum is displayed in blue. Literature values for different compounds are depicted as boxes.<sup>[31,32]</sup> Reproduced with permission.<sup>[27]</sup> Copyright 2018, American Chemical Society.

is altered (dependent on the particular treatment). Furthermore, changes in adsorbates and surface oxides are observed. Overall, the variations observed after the RbF PDT are expected to directly influence the electronic properties at the surface and the buffer/absorber interface, which will be discussed in Section 4 of this paper.

While best solar-cell efficiencies are usually achieved using a CdS buffer layer (deposited in a chemical bath), significant efforts are undertaken to replace CdS by a Cd-free, more transparent material which is compatible with an in-line production process. One very promising alternative material is indium sulfide ( $\text{In}_x\text{S}_y$  in the following), which, when doped with Na, has been successfully used by the Avancis GmbH for CIGSSe-based modules, reaching certified efficiencies of 17.9%<sup>[34]</sup> on an area of  $30 \times 30 \text{ cm}^2$ . Avancis deposits their dry  $\text{In}_x\text{S}_y$  buffer layer by a physical vapor deposition process, which can be integrated into an in-line production. Note that the Ga-concentration at the Avancis absorber surface is below the XPS detection limit, and hence we refer to this absorber as “CISSe”.

The XPS data of the as-deposited samples with varying buffer layer thickness with and without the addition of Na points towards an interface with a small degree of Cu diffusion from the absorber into the buffer layer.<sup>[35,36]</sup> Our XPS/XES study of

$\text{In}_2\text{S}_3$  layers from the Institut des Matériaux Jean Rouxel (IMN, University of Nantes) revealed a similar diffusion of Cu into the buffer.<sup>[37,38]</sup>

After  $\text{In}_x\text{S}_y$  deposition, an i-ZnO/n-ZnO transparent front contact is deposited at temperatures reaching 200 °C. To understand the impact of this additional thermal load, it was simulated in our experiment by annealing the buffer layer samples to 100 °C (for 30 min) and subsequently to 200 °C (for 30 min) under UHV conditions. We find that this strongly enhances the diffusion of Cu into the buffer layer,<sup>[35,36]</sup> and, furthermore, that this diffusion is considerably stronger for films without Na addition as compared to the Na-doped  $\text{In}_x\text{S}_y$  films.<sup>[35,39]</sup> To further analyze the compounds formed during the buffer layer deposition and the subsequent annealing process, samples were investigated using XES.

As described above, XES offers increased bulk sensitivity compared to XPS and allows studying the local chemical environment of a selected element. In the present case, we studied the S  $L_{2,3}$  emission of the absorber and  $\text{In}_x\text{S}_y$ /CISSe samples of different  $\text{In}_x\text{S}_y$  thicknesses, which is presented in Figure 5. All S  $L_{2,3}$  spectra are dominated by a peak at  $\approx 148 \text{ eV}$  (not shown in the spectral window in Figure 5), which is due to transitions from S 3s derived states to S 2p core holes, and hence indicates the (expected) presence of S in the samples. In contrast, the spectral features shown in Figure 5 all pertain to the valence band states of the investigated samples, and can be identified as follows. The spectrum of CISSe (Figure 5a) exhibits transitions from In 5s derived bands [(1), between 154 and 158.5 eV] and Cu 3d derived bands [(2), around 160 eV], both hybridized with S-derived valence states. The  $\text{In}_2\text{S}_3$  reference spectrum (Figure 5d) is characterized by a broad structure between 154 and 160 eV, which is also attributed to In 5s derived bands. The spectrum of the 10 nm thick buffer layer (Figure 5b) largely resembles that of the underlying absorber, but also contains  $\text{In}_2\text{S}_3$  contributions. The spectrum of the

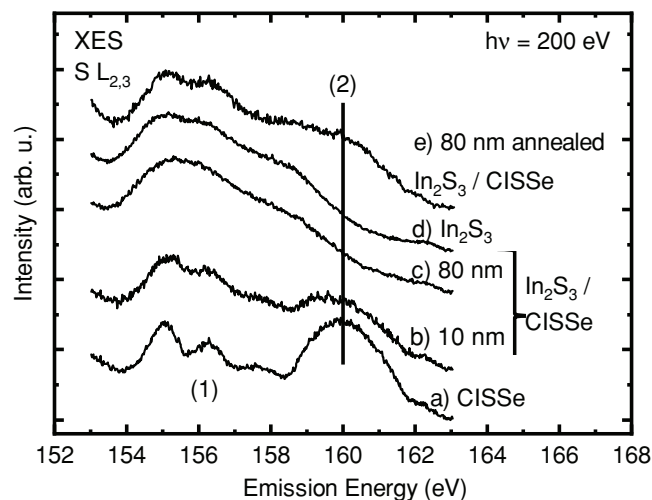


**Figure 5.** a) S  $L_{2,3}$  XES spectra of a CISSe film, two as-deposited  $\text{In}_2\text{S}_3$ /CISSe interface structures with b) 10, and c) 80 nm buffer layer thickness, d) an  $\text{In}_2\text{S}_3$  reference, and e) the 80 nm  $\text{In}_2\text{S}_3$ /CISSe sample after annealing at 200 °C. The features labeled (1) and (2) are discussed in the text. Reproduced with permission.<sup>[36]</sup> Copyright 2015, American Chemical Society.

80 nm thick buffer layer (Figure 5c) is, in contrast, dominated by the  $\text{In}_2\text{S}_3$  signature, indicating that spectral contributions from the substrate are essentially fully attenuated. As mentioned above, the additional thermal load of the window layer deposition, here simulated by an annealing step, leads to Cu diffusion into the buffer layer. This can also be derived from the XES spectra, where Figure 5e clearly shows a spectrum with contributions from S atoms in a  $\text{CuInS}_2$  environment, as can be seen in comparison with the absorber spectrum. The diffusion of Cu into the  $\text{In}_x\text{S}_y$  buffer layer likely leads to a further depletion of the absorber surface of Cu, creating a Cu concentration gradient, which has direct impact on the electronic properties at the interface.

#### 4. The Electronic Structure of Surfaces and Interfaces

Using XPS, XAES, and XES as powerful probes to derive a detailed picture of the chemical properties at surfaces and interfaces gives very helpful feedback to understand, e.g., the influence of surface treatments, diffusion processes, secondary phases, as well as (often unexpected) impurities. It is probably even more important to understand how these properties influence the electronic structure at the interface, which will directly influence electron transport and recombination and thus the efficiency of the solar cell.

Generally, we have been able to demonstrate that it is very important to use suitable experimental techniques that are able to *directly* determine the electronic properties (i.e., band edges relative to the Fermi level, valence and conduction band alignments, and the bandgap) *at the surface*. This is necessary since the chemical composition at the surface differs considerably from the bulk of the films and, as discussed above, often additional effects such as intermixing occur at the interface. As mentioned in the previous section, the surface of high-quality CIGSSe absorber is generally Cu poor, which directly influences the bandgap at the surface. Already early UPS experiments suggested a widening of the bandgap at the surface,<sup>[12]</sup> which we later directly confirmed by a combination of UPS and IPES.<sup>[10]</sup>

We recently added reflection electron energy loss spectroscopy (REELS) to our experimental tool chest for an independent determination of the bandgap at the CISSe surface and several  $\text{In}_2\text{S}_3$  buffer layers.<sup>[14]</sup> REELS also allows the determination of optical constants at the surface by illuminating the sample with electrons and measuring the number of reflected electrons with an electron analyzer as a function of kinetic energy. Beside elastically reflected electrons, electrons are detected that underwent an *inelastic* scattering process, having created an excitation in the sample, and now appearing at lower kinetic energies compared to the elastic line. The lowest possible energy for an electronic excitation in a (ground-state) semiconductor corresponds to the (excitonic) bandgap, which can thus be extracted from the REELS spectrum.

Figure 6a shows the REELS spectrum of an  $\text{In}_x\text{S}_y$  buffer layer from AVANCIS and the derived inelastic scattering cross-section. The cross-section is shown again in Figure 6b, together with the derived bandgap, and compared with an  $\text{In}_x\text{S}_y$  buffer layer after annealing (Figure 6c) and a CISSe absorber film

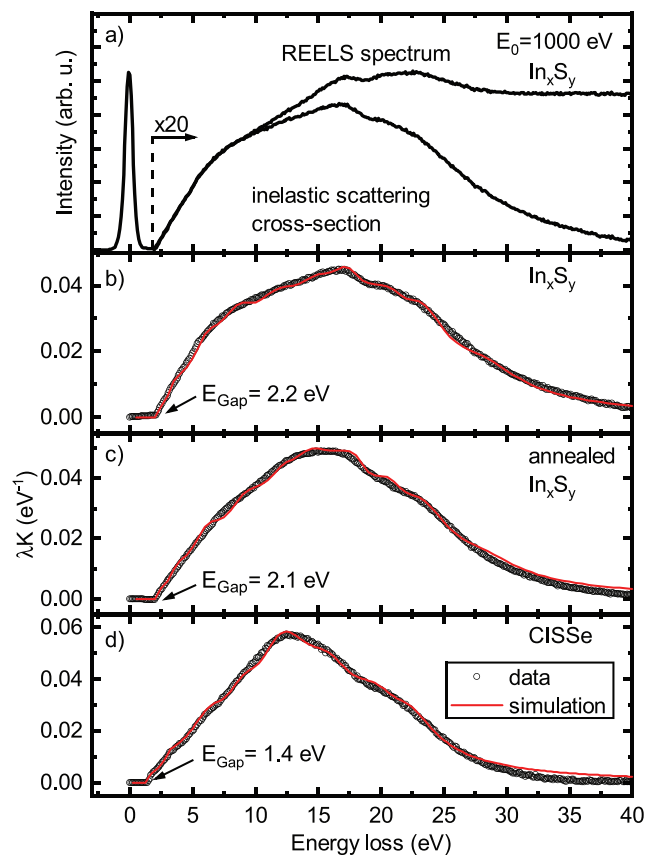


**Figure 6.** a) REELS spectrum and derived inelastic scattering cross-section of an indium sulfide buffer layer ( $E_0 = 1000$  eV). The inelastic region is magnified by a factor of 20. b–d) Comparison of inelastic scattering cross-sections  $\lambda K(E)$  of indium sulfide, annealed indium sulfide, and CISSe absorber (circles) with simulated spectra calculated with QUEELS- $\epsilon(k, \omega)$ -REELS software (red). The extracted bandgaps are indicated. Reproduced with permission.<sup>[14]</sup> Copyright 2016, American Chemical Society.

(Figure 6d). The surface bandgap of the films can be determined by a linear extrapolation of the leading edge of the inelastic scattering cross-section or by a simulation of the entire cross-section calculated with QUEELS- $\epsilon(k, \omega)$ -REELS software.<sup>[40]</sup> The latter is shown as red lines in Figure 6b–d. Both methods give the same result within the error bar (absolute bandgap values  $\pm 0.2$  eV, relative variations  $\pm 0.1$  eV).

For the CISSe absorber surface, we observe a bandgap of 1.4 eV, which is in good agreement with our earlier UPS/IPES studies<sup>[10,11]</sup> and significantly larger than the bulk bandgap of the absorber film (1.03 eV, as derived by bulk-sensitive reflection spectroscopy<sup>[41]</sup>). The reason for the increased bandgap is found in the increased S content and the Cu depletion generally found at the surface of high-efficiency absorbers.

For the unannealed  $\text{In}_x\text{S}_y$  buffer, we find a surface bandgap of  $(2.2 \pm 0.2)$  eV, in good agreement with reported values derived by optical spectroscopy,<sup>[42–44]</sup> which is then slightly reduced after the annealing (to  $2.1 \pm 0.2$  eV). This reduction is ascribed to the Cu diffusion discussed above, which is expected to lower the bandgap of the buffer layer. The values derived for the  $\text{In}_x\text{S}_y$  buffer using REELS agree (within the error bars)

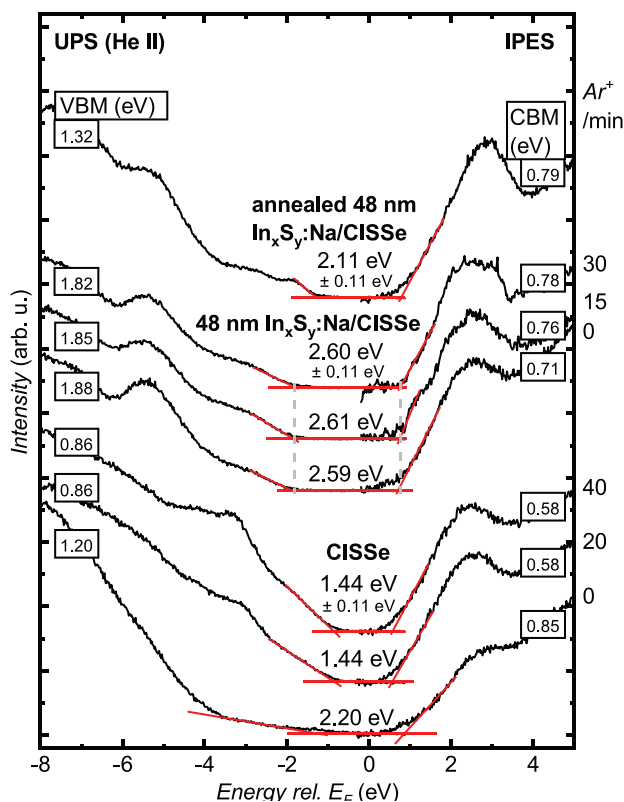


**Figure 7.** UPS and IPES data of CISSe, 48 nm In<sub>x</sub>S<sub>y</sub>:Na/CISSe, and annealed 48 nm In<sub>x</sub>S<sub>y</sub>:Na/CISSe. 50 eV Ar<sup>+</sup> ion treatment times are shown at the right margin (in minutes). The VBM ( $\pm 0.05$  eV) and CBM ( $\pm 0.10$  eV) are determined with a linear extrapolation of the leading edges, as indicated by red lines, and are given in the boxes at the margins of the graph. The respective resulting bandgaps ( $\pm 0.11$  eV) are listed in the center. Reproduced with permission.<sup>[35]</sup> Copyright 2018, Wiley.

with the results obtained by the combination of UPS and IPES:  $2.31 \pm 0.13$  eV for the unannealed In<sub>x</sub>S<sub>y</sub>, and  $1.94 \pm 0.13$  eV for the annealed In<sub>x</sub>S<sub>y</sub>.

The addition of Na to the buffer layer then leads to an increase of the bandgap and we find values of  $2.60 \pm 0.11$  eV for the unannealed In<sub>x</sub>S<sub>y</sub>:Na, and  $2.11 \pm 0.11$  eV for the annealed In<sub>x</sub>S<sub>y</sub>:Na buffer layers. This is derived from the various UPS (left) and IPES (right) spectra shown in **Figure 7** — a “bare” CISSe surface (after 0, 20, and 40 min of 50 eV Ar<sup>+</sup> ion treatment for surface cleaning), a 48 nm thick In<sub>x</sub>S<sub>y</sub>:Na buffer layer (after 0, 15, and 30 min of ion treatment), and the latter sample after annealing.

In addition to the determination of values for the bandgap at the sample surface, the UPS and IPES measurements in **Figure 7** allow to directly derive the positions of VBM and CBM with respect to the Fermi level. This is done by a linear extrapolation of the leading edge<sup>[45]</sup> of the respective spectra. The VBM and CBM positions can, in turn, be used to determine the band alignment at the interface. The values have to be corrected by the changes of band bending that occur due to the interface formation and the associated short- and long-range charge transfers in both the substrate and the overlayer (including the “interface dipole”). These changes (sometimes referred to as “interface-induced band bending”) can be measured by

monitoring the positions of the core levels of the substrate (here: the absorber film) and the overlayer (here: the In<sub>x</sub>S<sub>y</sub>:Na buffer layer) for the absorber, the thick buffer layer sample, and intermediate, thin buffer layer samples, for which both signals from the substrate and the overlayer can be detected. In the present case, the result of this band alignment analysis is shown for the unannealed system in **Figure 8a**. We find a spike ( $0.32 \pm 0.15$  eV) in the conduction band, which might act as a barrier for electron transport across the interface.

In the case of the *annealed* system, a straightforward correction of the interface-induced band bending is not possible, since the annealing step has to be performed with the full-thickness buffer layer, making it impossible to access the then hidden interface with the surface-sensitive electron spectroscopies. Nevertheless, the detailed characterization of the changes in chemical structure allows to qualitatively discuss the possible effect of these changes on the band alignment.<sup>[35]</sup> Following the above-discussed diffusion of Cu into the buffer layer, the expected corresponding Cu depletion at the (former) absorber surface will lead to an increase of its bandgap, which is illustrated in **Figure 8b** by the gray bars. Based on this, we speculate that the observed spike in the conduction band of the unannealed system is reduced, leading to a more favorable (flat) conduction band alignment, in agreement with the high efficiencies achieved with this buffer layer on large area devices.

Using the same combination of UPS, IPES, and XPS to determine VBM, CBM, and interface induced band bending we also determined the band alignment at the interface between CdS and (the above-discussed) RbF-treated CIGSe absorbers from ZSW.<sup>[24]</sup> As might be expected from the record efficiencies of the corresponding devices, we find a flat conduction band alignment with vanishing conduction band offset ( $0.03 \pm 0.16$  eV). An interesting observation is that the RbF treatment has only a small influence on the positions of VBM and CBM at the absorber surface but leads to a significant downward band bending induced by the interface formation after RbF treatment. Both, the flat alignment at the interface, as well as this additional downward band bending, are favorable for high efficiency devices to allow for an unimpeded electron transport and minimized interface recombination.<sup>[46,47]</sup>

## 5. Conclusion

Electron and X-ray spectroscopies are very powerful tools to study the chemical and electronic properties of state-of-the-art applied systems (e.g., thin-film solar cells). The particular strength of the approach lies in combining a toolbox of lab-based (i.e., XPS, XAES, UPS, IPES, and REELS) techniques with spectroscopy performed at synchrotron radiation sources (XES, XAS, and RIXS). Our results show that the properties at surfaces and interfaces differ from the bulk in terms of stoichiometry, secondary phases, and unexpected elements. We find that the chemical structure at the interfaces can be complex (including diffusion and intermixing effects) and very sensitive to the specific preparation parameters. All this underlines the importance of using techniques that allow to directly probe surfaces and interfaces. This is particularly important for the

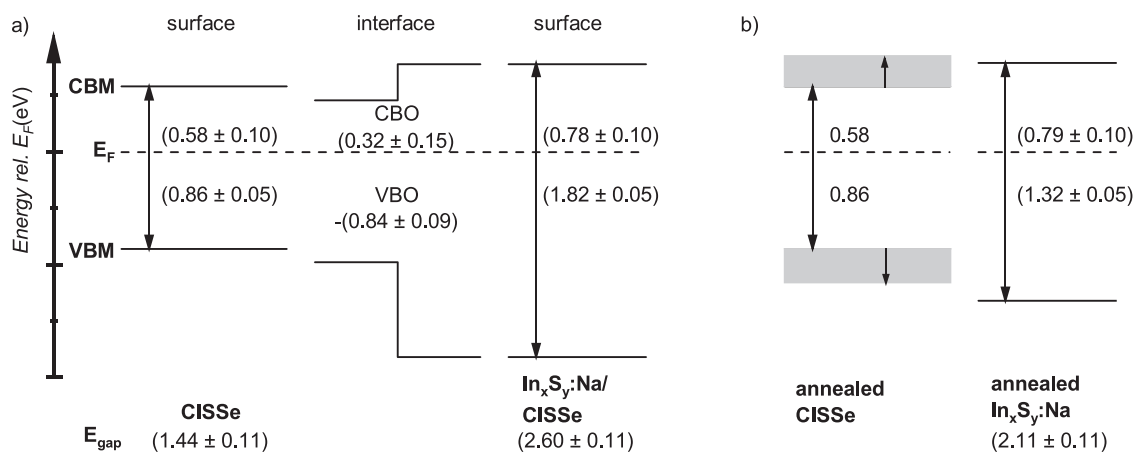


**Figure 8.** a) Schematic band diagrams of the as-deposited In<sub>x</sub>S<sub>y</sub>:Na/CISSe interface and b) the annealed interface. Electronic surface bandgaps are listed underneath the respective diagram. In b), the speculated “response” of the absorber bandgap to the annealing step is indicated by gray bars. All values are given in eV. Reproduced with permission.<sup>[35]</sup> Copyright 2018, Wiley.

determination of valence and conduction band offsets, which are crucial for the electron transport across the interfaces.

Using this experimental approach, it was possible to paint a detailed picture of the processes that occur during the alkali fluoride PDT of the absorber surface as well as the interface involving alternative In<sub>x</sub>S<sub>y</sub> buffer layers, both of which are current topics with high relevance for record efficiencies on a laboratory scale and for large area modules. After alkali fluoride PDT, we find alkali elements at the absorber surface and a reduction of the Cu content. RbF PDT leads to a beneficial additional downward band bending in the absorber.

For In<sub>x</sub>S<sub>y</sub> buffer layers, we find strong diffusion of Cu into the buffer layer after a heat treatment. This diffusion is reduced upon addition of Na to the buffer and reduces or removes a spike in the conduction band alignment in accordance with the observed improvement in the solar-cell efficiency.

Thus, electron and soft X-ray techniques prove to be very powerful for the investigation of surfaces and interfaces in thin-film solar cells. Recently, strong efforts have been undertaken to apply some of these techniques to in situ environments as well, and we have begun to also use such approaches to study thin-film solar cells. This will add a valuable point of view for the optimization of cell stability under different atmospheres and during thin-film deposition, e.g., in a chemical bath.

## Acknowledgements

The authors are grateful for financial support by the German Federal Ministry for Economic Affairs and Energy, BMWi, under project “EFFCIS” (No. 0324076E) as well as the German Federal Ministry of Education and Research, BMBF (Free-InCa, 03SF0530B). This research used resources of the Advanced Light Source, which is a DOE Office of Science User Facility under contract no. DE-AC02-05CH11231.

## Conflict of Interest

The authors declare no conflict of interest.

## Keywords

chemical structures, electronic structures, surface characterization, thin-film solar cells

Received: October 14, 2018

Revised: December 9, 2018

Published online: February 21, 2019

- [1] M. A. Green, Y. Hishikawa, E. D. Dunlop, D. H. Levi, J. Hohl-Ebinger, A. W. Y. Ho-Baillie, *Prog. Photovoltaics* **2018**, *26*, 427.
- [2] A. Chirilă, P. Reinhard, F. Pianezzi, P. Bloesch, A. R. Uhl, C. Fella, L. Kranz, D. Keller, C. Gretener, H. Hagendorfer, D. Jaeger, R. Erni, S. Nishiwaki, S. Buecheler, A. N. Tiwari, *Nat. Mater.* **2013**, *12*, 1107.
- [3] P. Jackson, R. Wuerz, D. Hariskos, E. Lotter, W. Witte, M. Powalla, *Physica Status Solidi—Rapid Res. Lett.* **2016**, *10*, 583.
- [4] Solar Frontier Achieves World Record Thin-Film Solar Cell Efficiency of 22.9% can be found under, [http://www.solar-frontier.com/eng/news/2017/1220\\_press.html](http://www.solar-frontier.com/eng/news/2017/1220_press.html) (accessed: 2017).
- [5] M. P. Seah, W. A. Dench, *Surf. Interface Anal.* **1979**, *1*, 2.
- [6] S. Tanuma, C. J. Powell, D. R. Penn, *Surf. Interface Anal.* **1994**, *21*, 165.
- [7] O. Fuchs, L. Weinhardt, M. Blum, M. Weigand, E. Umbach, M. Bär, C. Heske, J. Denlinger, Y. D. Chuang, W. McKinney, Z. Hussain, E. Gullikson, M. Jones, P. Batson, B. Nelles, R. Follath, *Rev. Sci. Instrum.* **2009**, *80*, 063103.
- [8] R. Qiao, Q. Li, Z. Zhuo, S. Sallis, O. Fuchs, M. Blum, L. Weinhardt, C. Heske, J. Pepper, M. Jones, A. Brown, A. Spucce, K. Chow, B. Smith, P.-A. Glans, Y. Chen, S. Yan, F. Pan, L. F. J. Piper, J. Denlinger, J. Guo, Z. Hussain, Y.-D. Chuang, W. Yang, *Rev. Sci. Instrum.* **2017**, *88*, 033106.
- [9] M. Blum, L. Weinhardt, O. Fuchs, M. Bär, Y. Zhang, M. Weigand, S. Krause, S. Pookpanratana, T. Hofmann, W. Yang, J. D. Denlinger, E. Umbach, C. Heske, *Rev. Sci. Instrum.* **2009**, *80*, 123102.
- [10] M. Morkel, L. Weinhardt, B. Lohmüller, C. Heske, E. Umbach, W. Riedl, S. Zweigart, F. Karg, *Appl. Phys. Lett.* **2001**, *79*, 4482.
- [11] L. Weinhardt, M. Morkel, T. Gleim, S. Zweigart, T. P. Niesen, F. Karg, C. Heske, E. Umbach, in *17th European Photovoltaic Solar Energy Conference*, WIP - Renewable Energies, Munich, Germany **2001**, p. 1261.
- [12] D. Schmid, M. Ruckh, F. Grunwald, H. W. Schock, *J. Appl. Phys.* **1993**, *73*, 2902.



- [13] D. Schmid, M. Ruckh, H. W. Schock, *Appl. Surf. Sci.* **1996**, *103*, 409.
- [14] D. Hauschild, E. Handick, S. Göhl-Gusenleitner, F. Meyer, H. Schwab, A. Benkert, S. Pohlner, J. Palm, S. Tougaard, C. Heske, L. Weinhardt, F. Reinert, *ACS Appl. Mater. Interfaces* **2016**, *8*, 21101.
- [15] L. Weinhardt, M. Bär, H. Muffler, C. H. Fischer, M. C. Lux-Steiner, T. P. Niesen, F. Karg, T. Gleim, C. Heske, E. Umbach, *Thin Solid Films* **2003**, *431–432*, 272.
- [16] L. Weinhardt, O. Fuchs, D. Gross, G. Storch, E. Umbach, N. G. Dhere, A. A. Kadam, S. S. Kulkarni, C. Heske, *Appl. Phys. Lett.* **2005**, *86*, 062109.
- [17] V. Probst, J. Rimmasch, W. Riedl, W. Stetter, J. Holz, H. Harms, F. Karg, H. W. Schock, in *First World Conference on Photovoltaic Energy Conversion (WCPEC)*, IEEE Electron Devices Society, Waikoloa **1994**, p. 144.
- [18] C. Heske, R. Fink, E. Umbach, W. Riedl, F. Karg, *Appl. Phys. Lett.* **1996**, *68*, 3431.
- [19] C. Heske, D. Eich, R. Fink, E. Umbach, S. Kakar, T. van Buuren, C. Bostedt, L. J. Terminello, M. M. Grush, T. A. Callcott, F. J. Himpsel, D. L. Ederer, R. C. C. Perera, W. Riedl, F. Karg, *Appl. Phys. Lett.* **1999**, *75*, 2082.
- [20] C. Heske, G. Richter, Z. Chen, R. Fink, E. Umbach, W. Riedl, F. Karg, *J. Appl. Phys.* **1997**, *82*, 2411.
- [21] M. Ruckh, D. Schmid, M. Kaiser, R. Schäffler, T. Walter, H. W. Schock, *Solar Energy Mater. Solar Cells* **1996**, *41–42*, 335.
- [22] C. Heske, D. Eich, U. Groh, R. Fink, E. Umbach, T. van Buuren, C. Bostedt, N. Franco, L. J. Terminello, M. M. Grush, T. A. Callcott, F. J. Himpsel, D. L. Ederer, R. C. C. Perera, W. Riedl, F. Karg, *Thin Solid Films* **2000**, *361–362*, 360.
- [23] C. Heske, D. Eich, R. Fink, E. Umbach, T. van Buuren, C. Bostedt, S. Kakar, L. J. Terminello, M. M. Grush, T. A. Callcott, F. J. Himpsel, D. L. Ederer, R. C. C. Perera, W. Riedl, F. Karg, *Surf. Interface Anal.* **2000**, *30*, 459.
- [24] D. Hauschild, D. Kreikemeyer-Lorenzo, P. Jackson, T. M. Friedlmeier, D. Hariskos, F. Reinert, M. Powalla, C. Heske, L. Weinhardt, *ACS Energy Lett.* **2017**, *2*, 2383.
- [25] M. Mezher, L. M. Mansfield, K. Horsley, M. Blum, R. Wieting, L. Weinhardt, K. Ramanathan, C. Heske, *Appl. Phys. Lett.* **2017**, *111*, 071601.
- [26] E. Handick, P. Reinhard, R. G. Wilks, F. Pianezzi, T. Kunze, D. Kreikemeyer-Lorenzo, L. Weinhardt, M. Blum, W. Yang, M. Gorgoi, E. Ikenaga, D. Gerlach, S. Ueda, Y. Yamashita, T. Chikyow, C. Heske, S. Buecheler, A. N. Tiwari, M. Bär, *ACS Appl. Mater. Interfaces* **2017**, *9*, 3581.
- [27] D. Kreikemeyer-Lorenzo, D. Hauschild, P. Jackson, T. Magorian-Friedlmeier, D. Hariskos, M. Blum, W. Yang, F. Reinert, M. Powalla, C. Heske, L. Weinhardt, *ACS Appl. Mater. Interfaces* **2018**, *10*, 37602.
- [28] B. Ürsür, W. Calvet, A. Steigert, I. Laueremann, M. Gorgoi, K. Prietzel, D. Greiner, C. A. Kaufmann, T. Unold, M. C. Lux-Steiner, *Phys. Chem. Chem. Phys.* **2016**, *18*, 14129.
- [29] J. A. Aguiar, A. Stokes, C.-S. Jang, T. Aoki, P. G. Kotula, M. K. Patel, B. Gorman, M. Al-Jassim, *Adv. Mater. Interfaces* **2016**, *3*, 1600013.
- [30] P. Pistor, D. Greiner, C. A. Kaufmann, S. Brunken, M. Gorgoi, A. Steigert, W. Calvet, I. Laueremann, R. Klenk, T. Unold, M.-C. Lux-Steiner, *Appl. Phys. Lett.* **2014**, *105*, 063901.
- [31] A. Naumkin, A. Kraut-Vass, S. Gaarenstroom, C. Powell, NIST X-ray Photoelectron Spectroscopy (XPS) Database, Version 4.1, can be found under, <http://srdata.nist.gov/xps/Default.aspx> (accessed: 2018).
- [32] J. F. Moulder, W. F. Stickle, P. E. Sobol, K. D. Bomben, in *Handbook of X-Ray Photoelectron Spectroscopy*, Perkin-Elmer Corporation; Physical Electronics Division, Eden Prairie, MN **1992**.
- [33] T. M. Friedlmeier, P. Jackson, D. Kreikemeyer-Lorenzo, D. Hauschild, O. Kiowski, D. Hariskos, L. Weinhardt, C. Heske, M. Powalla, in *2016 IEEE 43rd Photovoltaic Specialists Conference (PVSC)*, Portland, OR **2016**, p. 0457.
- [34] Module with record efficiency from AVANCIS: Fraunhofer ISE certifies CIGS solar module with an efficiency of 17.9%, can be found under, <https://www.avancis.de/en/press/news/article/avancis-erzielt-erneuten-wirkungsgradrekord-fraunhofer-ise-zertifiziert-cigs-solarmodul-mit-wirkung/> (accessed: January 2019).
- [35] D. Hauschild, F. Meyer, A. Benkert, D. Kreikemeyer-Lorenzo, T. Dalibor, J. Palm, M. Blum, W. Yang, R. G. Wilks, M. Bär, F. Reinert, C. Heske, L. Weinhardt, *Prog. Photovoltaics* **2018**, *26*, 359.
- [36] D. Hauschild, F. Meyer, A. Benkert, D. Kreikemeyer-Lorenzo, S. Pohlner, J. Palm, M. Blum, W. Yang, R. G. Wilks, M. Bär, C. Heske, L. Weinhardt, F. Reinert, *J. Phys. Chem. C* **2015**, *119*, 10412.
- [37] M. Bär, N. Barreau, F. Couzinié-Devy, L. Weinhardt, R. G. Wilks, J. Kessler, C. Heske, *ACS Appl. Mater. Interfaces* **2016**, *8*, 2120.
- [38] M. Bär, N. Barreau, F. Couzinié-Devy, S. Pookpanratana, J. Klaer, M. Blum, Y. Zhang, W. Yang, J. D. Denlinger, H.-W. Schock, L. Weinhardt, J. Kessler, C. Heske, *Appl. Phys. Lett.* **2010**, *96*, 184101.
- [39] D. Hauschild, F. Meyer, A. Benkert, T. Dalibor, P. Eraerds, J. Palm, R. G. Wilks, M. Bär, M. Blum, W. Yang, F. Reinert, C. Heske, L. Weinhardt, in *World Conference on Photovoltaic Energy Conversion (WCPEC-7)*, IEEE Electron Devices Society, Waikoloa **2018**.
- [40] S. Tougaard, *QUASES (QUantitative Analysis of Surfaces by Electron Spectroscopy)*, <http://www.Quases.Com/Home/> (accessed: 2016).
- [41] F. Karg, H. Vogt, A. Heiß, R. Dietmüller, R. Verma, S. Pohlner, R. Lechner, T. Dalibor, J. Palm, in *29th European Photovoltaic Solar Energy Conference and Exhibition*, WIP, Amsterdam **2014**, p. 1433.
- [42] N. Barreau, J. C. Bernède, S. Marsillac, *J. Cryst. Growth* **2002**, *241*, 51.
- [43] J. Sterner, J. Malmström, L. Stolt, *Prog. Photovoltaics* **2005**, *13*, 179.
- [44] M. Richter, C. Schubert, P. Eraerds, I. Riedel, J. Keller, J. Parisi, T. Dalibor, A. Avellán-Hampe, *Thin Solid Films* **2013**, *535*, 331.
- [45] T. Gleim, C. Heske, E. Umbach, C. Schumacher, S. Gundel, W. Faschinger, A. Fleszar, C. Ammon, M. Probst, H.-P. Steinrück, *Surf. Sci.* **2003**, *531*, 77.
- [46] R. Klenk, *Thin Solid Films* **2001**, *387*, 135.
- [47] T. Minemoto, T. Matsui, H. Takakura, Y. Hamakawa, T. Negami, Y. Hashimoto, T. Uenoyama, M. Kitagawa, *Solar Energy Mater. Solar Cells* **2001**, *67*, 83.